

In-Medium Vector Mesons, Dileptons and Chiral Restoration

Ralf Rapp

Cyclotron Institute and Department of Physics & Astronomy, Texas A&M University, College Station, TX 77843-3366, USA

Abstract. Medium modifications of the electromagnetic spectral function in hadronic and quark-gluon matter are reviewed. A strong broadening of the ρ meson, which dominates the spectral function in the low-mass regime, is quantitatively consistent with dilepton excess spectra measured in photoproduction off cold nuclei (CLAS/JLab) and in fixed-target ultrarelativistic heavy-ion collisions (NA45, NA60/CERN-SPS). The large excess observed by PHENIX at RHIC remains unexplained to date, but is most likely not due to emission from the Quark-Gluon Plasma. Connections to thermal lattice QCD promise progress in the search for chiral symmetry restoration.

Keywords: Medium Modifications of Hadrons, Dileptons, Relativistic Heavy-Ion Collisions

INTRODUCTION

The vacuum of Quantum Chromodynamics (QCD) is very dense, filled with condensates made of composite quark and gluon configurations. These condensates are believed to be at the origin of two of the most prominent nonperturbative phenomena of the strong interaction, namely the generation of hadronic masses and the confinement of color charge. For example, the formation of the chiral quark condensate, $\langle 0 | \bar{q}q | 0 \rangle \simeq -2 \text{ fm}^{-3}$ per light quark flavor (u , d and maybe s), breaks the chiral invariance of the QCD Lagrangian and generates constituent light-quark masses of $m_{u,d} \simeq 350 \text{ MeV}$, compared to the bare quark masses of $m_{u,d}^0 \simeq 5\text{-}10 \text{ MeV}$ in the Lagrangian. The origin of confinement is less well understood; an intuitive (and theoretically viable [1]) picture is that of a dual superconductor, where the condensation of color-magnetic monopoles forces color-electric into quasi-one-dimensional configurations, the color-electric flux tubes (strings) generating the confining potential between two static color charges.

Since condensates are not directly observable, one has to infer their presence and properties via their excitations. In the QCD vacuum these are nothing but the hadron spectrum. A particularly instructive example is the vector ($J^{PC} = 1^{--}$) spectral function which is accurately measured in electron-positron annihilation into hadrons, see left panel in Fig. 1¹. The upper panel nicely illustrates a decomposition into a nonperturbative regime at masses below $\sim 1.5 \text{ GeV}$ and a perturbative regime above. In the former, the spectral strength is concentrated in the formation of the low-mass vector mesons (ρ , ω and ϕ) with dynamical mass while the latter is characterized by a continuum shape

¹ The vector and electromagnetic (EM) correlation functions essentially differ by a factor of the electric charge squared, e^2 .

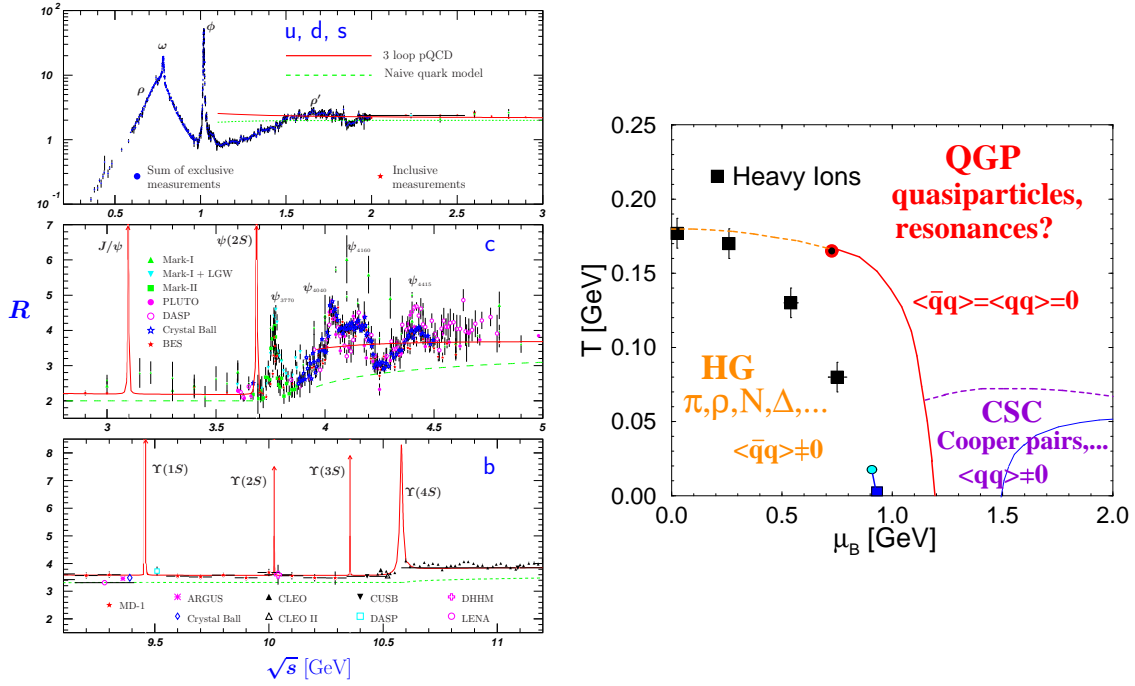


FIGURE 1. Left panel: data compilation [2] of the cross-section ratio $R = \sigma(e^+e^- \rightarrow \text{hadrons})/\sigma(e^+e^- \rightarrow \mu^+\mu^-)$ as a function of center-of-mass energy. Right panel: Schematic diagram of the phase structure of QCD indicating hadronic matter at low temperature (T) and baryon chemical potential (μ_B), and transitions into a Quark-Gluon Plasma (QGP) at high T and into Color-Super-Conducting (CSC) phases at high μ_B (small T). For each of these 3 regions the lowest dimension quark condensates and expected degrees of freedom are indicated. The idea is to infer these properties by using the vector spectral function shown in the left panel as a probe.

whose strength coincides with that of a perturbative $q\bar{q}$ final state (the subsequent formation of the multi-hadron final state appears to have little impact on the cross section)². An analogous pattern is observed in the spacelike regime (negative $q^2 \equiv -Q^2$), as probed, e.g., in electron scattering off the proton: JLab data for the F_2^p structure function [3] show a gradual transition from a nucleon-resonance dominated regime at low Q^2 to a structureless (perturbative) continuum for $Q^2 \geq 3 \text{ GeV}^2$, in agreement with the universal form measured in deep-inelastic scattering (DIS).

A central objective in nuclear physics is the exploration of matter aggregates governed by the strong force, i.e., its phase diagram, schematically depicted in the right panel of Fig. 1. At high temperature (and baryon chemical potential) asymptotic freedom of QCD predicts the bulk medium to be a weakly interacting plasma of quarks and gluons (modulo colorsuperconducting quark pairing at a cold Fermi surface). Thus, hadronic spectral functions should be close to their perturbative form, with no more resonant correlations. For the vector spectral function shown in Fig. 1 this implies that the

² In the vicinity of the charm-anticharm (middle panel) and bottom-antibottom thresholds (lower panel), heavy quarkonium bound states (Ψ and Y families) prevail, encoding information on the confining force.

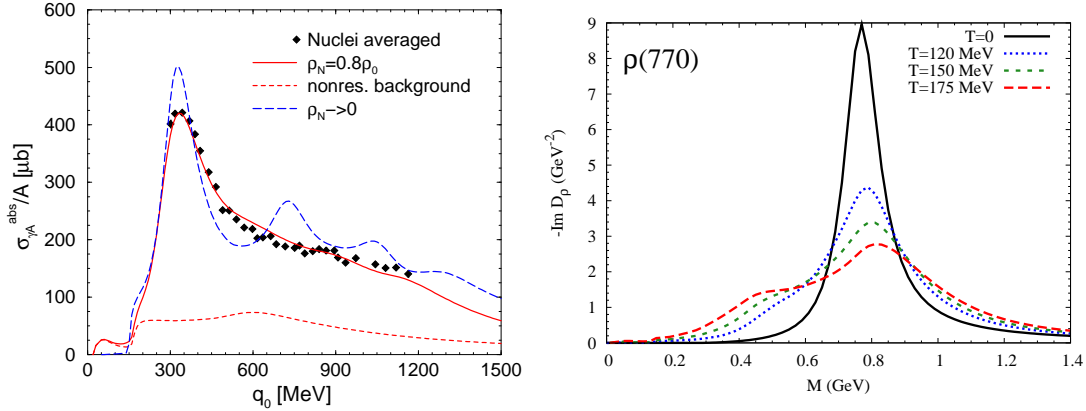


FIGURE 2. Left panel: constraints on the ρ -meson coupling to nucleons by applying the light-like ρ spectral function, $\text{Im} D_\rho(q_0 = q, \rho_N)$, to calculate total photoabsorption cross sections on the nucleon (low-density limit, long-dashed line) and on nuclei (solid line, for $\rho_N = 0.8\rho_0$; short-dashed line: contribution from the in-medium pion cloud) [6]. The data are averaged over nuclei from Li to Pb (stat. error below 2%). Right panel: in-medium ρ -meson spectral function [8] under conditions associated with heavy-ion collisions at the SPS; baryon-density effects are dominant, with $\rho_B \simeq 1.5(0.5)\rho_0$ at $T=175(120)$ MeV.

resonance peaks have melted into a structureless continuum (signaling chiral restoration and deconfinement). A key question is how this transition is realized, in particular when passing through phase changes of the medium. This is the main idea of vector-meson spectroscopy of hot and dense matter. The vector channel is unique since it directly couples to (real and virtual) photons which can carry undistorted spectral information from the interior of strongly interacting systems in the laboratory (nuclei, heavy-ion collisions): the EM mean-free-path is much larger than the system size, $\lambda_{\text{em}} \gg R_{\text{nucleus}}$.

In the following sections we review calculations of ρ -meson spectral functions in hot and dense hadronic matter, discuss their applications to dilepton production experiments in photon-nucleus and ultrarelativistic heavy-ion collisions (URHICs), and elaborate connections to thermal lattice QCD. The final section contains conclusions.

VECTOR MESONS IN VACUUM AND IN MEDIUM

Starting point for the description of vector-meson spectral function in hadronic matter is a realistic model in vacuum. For the ρ -meson, on which we will focus here, this requires to compute its coupling to 2-pion states to properly describe P -wave $\pi\pi$ phase shifts and the pion EM formfactor in the timelike regime [6, 7].

Medium modifications of the ρ propagator, $D_\rho = [M^2 - (m_\rho^0)^2 - \Sigma_{\rho\pi\pi} - \Sigma_{\rho B, M}]^{-1}$, are calculated via selfenergy insertions corresponding to a dressing of its pion cloud ($\Sigma_{\rho\pi\pi}$) and direct couplings to the mesons ($\Sigma_{\rho M}$) and baryons ($\Sigma_{\rho B}$) in the heat bath (see Refs. [4, 5] for recent reviews). To fix the coupling constants and formfactors of resonance excitations, empirical constraints from their decay branchings and scattering data are essential, e.g., using total photoabsorption cross sections on the nucleon and nuclei [6], cf. left panel of Fig. 2. The resulting ρ spectral function, $\text{Im} D_\rho$, strongly

broadens in the medium, approximately doubling (tripling) its free width in cold nuclear matter at half (full) saturation density ($\rho_0 = 0.16 \text{ fm}^{-3}$). Under conditions expected in heavy-ion collisions at the CERN-SPS, the ρ resonance “melts” (i.e., $\Gamma_\rho \rightarrow m_\rho$) when extrapolated into the putative phase transition region (see right panel of Fig. 2), mostly driven by the baryonic component of the medium. This remains true at RHIC, despite the low net-baryon density at mid-rapidities, due to an appreciable density of baryons *plus* antibaryons.

DILEPTON PHENOMENOLOGY

Recent experiments have made major progress in extracting so-called “excess” dilepton spectra, which can be directly compared to theoretical calculations of the in-medium signal. This has been achieved in both nuclear photoproduction at JLab [9] (probing cold nuclear matter at $\rho_N \approx 0.5\rho_0$) and in URHICs at the SPS [10, 11, 12] (probing hot and dense hadronic matter at $(\rho_B, T) \approx (\rho_0, 150 \text{ MeV})$). The main difference in the theoretical description of these experiments lies in the excitation mechanism. In URHICs, the large amount of incoming kinetic energy is quickly randomized producing a locally equilibrated (macroscopic) source, justifying the simplifying notion of thermal emission. In reactions with an elementary projectile (e.g., photon), the ρ production process requires a microscopic calculation (e.g., $\gamma N \rightarrow \rho N$ amplitude), while the subsequent in-medium propagation may be approximated assuming zero-temperature nuclear matter.

Nuclear Photoproduction: Spectra and Absorption

The CLAS experiment at JLab [9] used photon Bremsstrahlung of energies $E_\gamma \simeq 1\text{--}3.5 \text{ GeV}$ to illuminate nuclear targets and measure e^+e^- spectra for $M_{ee} \simeq 0.2\text{--}1.2 \text{ GeV}$. After subtraction of the background and the narrow ω and ϕ peaks, the excess spectra were fitted with a schematic ρ -meson spectral function. For Fe-Ti targets, an average width of $\Gamma_\rho \simeq (220 \pm 15) \text{ MeV}$ was extracted, without significant mass shift.

A calculation [13] of the CLAS excess spectra using a realistic $\gamma N \rightarrow \rho N$ production amplitude [14] coupled to in-medium ρ propagation and decay [8] is shown in Fig. 3. The moderate broadening of the line shape seen in the data is reasonably well reproduced without (re-) adjusting parameters. This may seem surprising given the large broadening of low-momentum ρ mesons in nuclear matter as quoted above. However, the relatively large ρ 3-momenta relative to the nucleus ($q \simeq 1.5 \text{ GeV}$, inherited from the incoming photon energies) cause a reduction of medium effects since (a) a significant portion of ρ 's decay outside (or in the surface region) of the nucleus, leading to average densities at the decay point of $\bar{\rho} \simeq 0.4\rho_0$ for ^{56}Fe , and (b) the broadening of the spectral function decreases with increasing 3-momentum [8]. The significance of the medium effects can be quantified by a χ^2 per data point of 1.08 when using the in-medium spectral function, compared to 1.55 for the vacuum one. A complementary assessment of their magnitude can be obtained from the nuclear transparency ratio, $T_A = \sigma_{\gamma A \rightarrow \rho X} / A \sigma_{\gamma N \rightarrow \rho X}$, which reflects the absorptive width of the ρ when traveling through the nucleus. The predictions shown in the right panel of Fig. 3 show a nuclear absorption by 40% for $A \simeq 200$ nuclei,

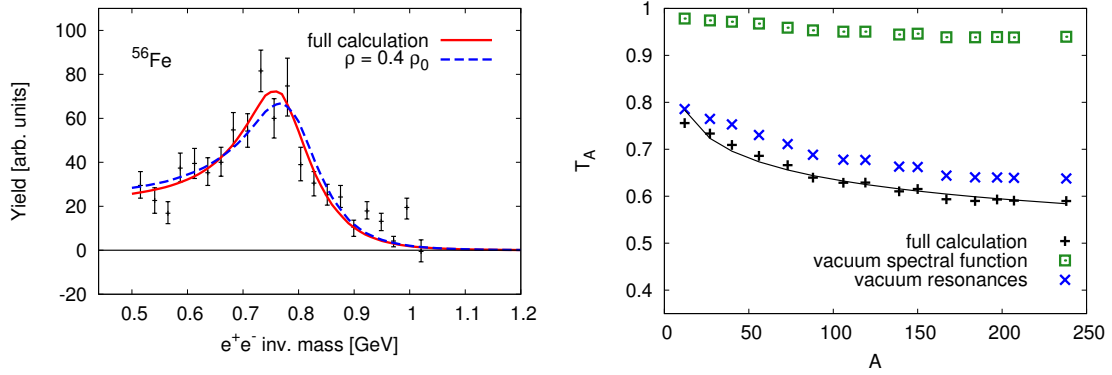


FIGURE 3. Nuclear photoproduction of dileptons [13] from ρ decays employing the in-medium propagator of Fig. 2 coupled with a realistic amplitude [14] for the elementary $\gamma + N \rightarrow \gamma + \rho$ production process. Left panel: invariant-mass spectra compared to CLAS data [9]; right panel: predictions for the nuclear transparency ratio as a function of nuclear mass number.

which is markedly less than what has been observed for ϕ and ω mesons [15, 16]. The reason for this difference is not a smaller ρ broadening in medium (in fact, it is larger), but its large width in the vacuum, or rather the “anomalously” small vacuum width of ω and ϕ (figuring into the denominator of T_A).

Heavy-Ion Collisions: Thermal Radiation

For the first time in heavy-ion collisions, the NA60 collaboration has recently achieved to extract a fully acceptance corrected *invariant*-mass spectrum of the observed dimuon-excess radiation in In-In collisions at the SPS (after subtraction of background and final-state hadron decays) [12], cf. upper right panel in Fig. 4 (a further improved version of this spectrum can be found in Ref. [17]). Theoretical calculations employing the in-medium ρ spectral function of Fig. 2, convoluted over an expanding fireball model, compare well to the data [18] (see also Refs. [19, 20, 21]). The calculations are absolutely normalized and contain one main parameter, the fireball lifetime ($\tau_{\text{FB}} \simeq 6 \pm 1 \text{ fm}/c$), which governs the total yield in the spectrum. The shape of the spectrum is determined by the predicted in-medium ρ spectral function at low mass ($M \leq 1 \text{ GeV}$), and by continuum-like emission from the QGP and multi-pion fusion at intermediate mass ($M > 1 \text{ GeV}$), with fixed relative strength. An important point here is that the Lorentz-invariant nature of the M -spectra eliminates any distortion from the collective expansion of the medium (pertinent blue shifts are known to strongly affect p_t -spectra of observed hadrons). This warrants a direct comparison of the experimental M -spectra to the theoretical input rates,

$$\frac{dN}{d^4x dM} = -\frac{\alpha_{\text{em}}^2}{\pi^3} \frac{L(M)}{M} \int \frac{d^3q}{q_0} f^B(q_0; T) \frac{1}{3} g_{\mu\nu} \text{Im} \Pi_{\text{em}}^{\mu\nu}(M, q; \mu_B, T), \quad (1)$$

which merely differ by the total four-volume of the expansion and the fact that the rates are for fixed temperature, while the spectra are convoluted over it. Since higher masses

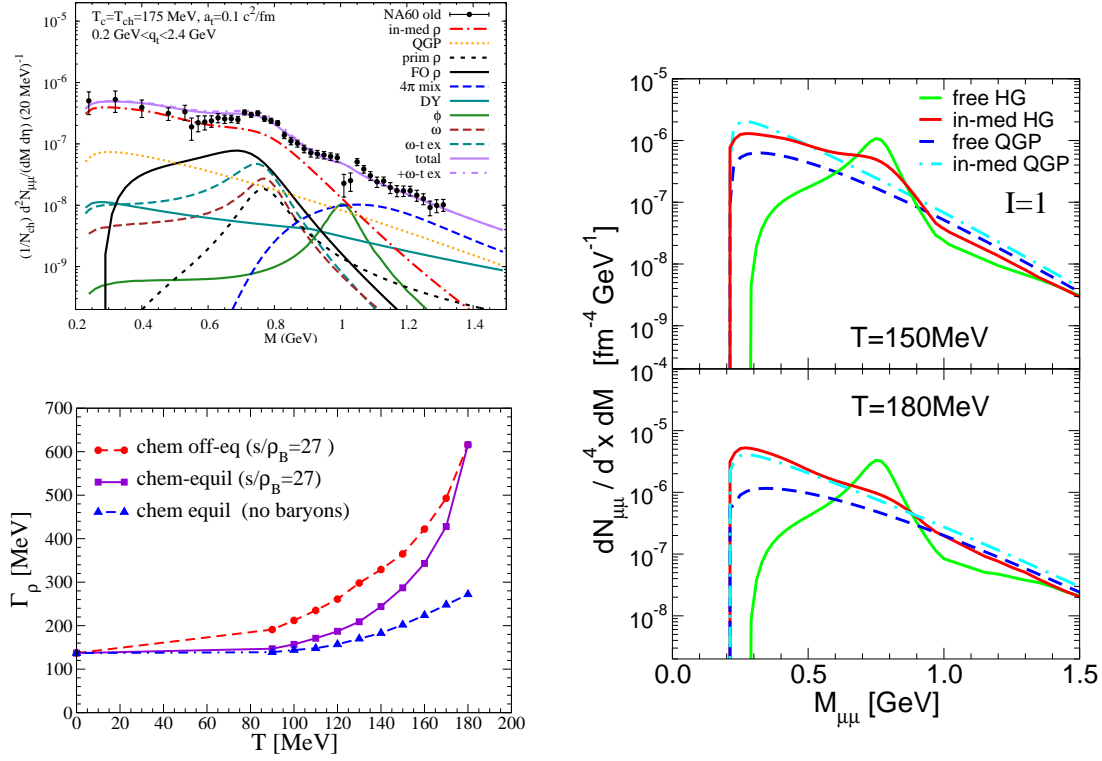


FIGURE 4. Upper left: Comparison of theoretical calculations of dilepton invariant-mass spectra [18] to fully acceptance-corrected dimuon-excess spectra in In(158 AGeV)-In collisions. Thermal sources (ρ decays at low mass, multi-pion annihilation and QGP emission at intermediate mass) dominate over non-thermal contributions. Lower left: evolution of the ρ width (circles) underlying the spectra in the upper panel, compared to chemical equilibrium (squares) and when switching off interactions with baryons (triangles) [4]. Right panel: 3-momentum integrated thermal dimuon emission rates for isovector hadronic (solid red lines) [8] and QGP emission (dash-dotted lines) [22] underlying the thermal spectra in the upper left, compared to free hadronic and $q\bar{q}$ rates.

are more sensitive to earlier temperatures, one expects a larger average temperature to contribute at $M \simeq 1.5$ GeV than at $M \simeq 0.3$ GeV. Indeed, when evaluating the ratio of the spectrum for these masses, $\frac{dN}{dM}|_{0.3\text{GeV}}/\frac{dN}{dM}|_{1.5\text{GeV}}$, one obtains about ~ 100 , which is quite close to the ratio of the emission rate taken for $T = 150$ MeV at $M \simeq 0.3$ GeV and for $T = 180$ MeV at $M \simeq 1.5$ GeV. The lower left panel of Fig. 4 shows the ρ width as it evolves in the medium at SPS (assumed to be in local thermal equilibrium). From the M -spectra one extracts an average value of $\bar{\Gamma}_\rho^{\text{med}} \simeq \Gamma_\rho(\rho_B = \rho_0, T = 150\text{MeV}) \simeq 350\text{--}400$ MeV, about 3 times the vacuum value. Given that roughly half of the radiation emanates from even higher (ρ_B, T) (as required, e.g., by the excess at $M > 1$ GeV), it is inevitable to conclude that the ρ resonance indeed melts.

Applying the same approach to di-electron spectra in Au-Au collisions at a factor of ~ 10 higher collision energies ($\sqrt{s} = 200$ AGeV at RHIC) leads to failure in comparison to recent PHENIX data [23], cf. left panel of Fig. 5. At first one might think that the difference arises from the factor of ~ 2 higher initial temperatures at RHIC ($T_0 \simeq 2T_c$)

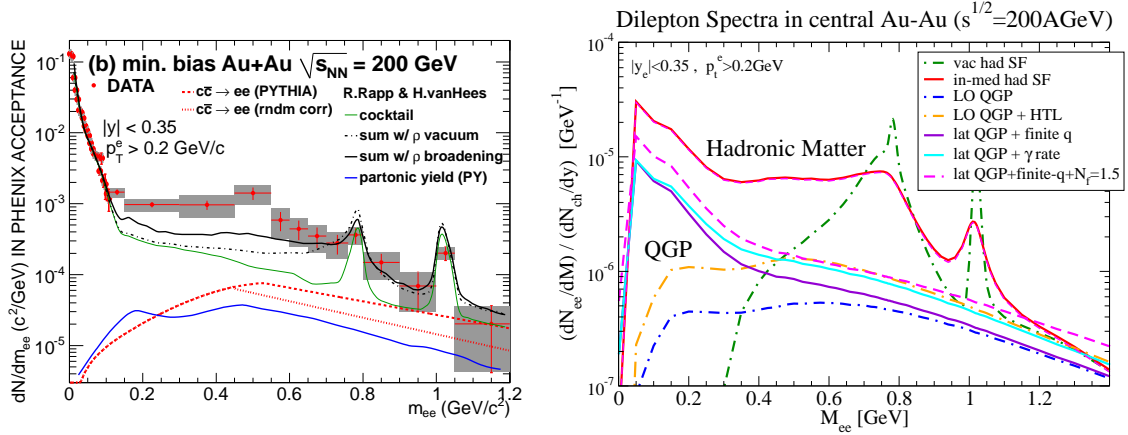


FIGURE 5. Left panel: theoretical calculations of thermal dilepton spectra in Au-Au collisions at RHIC using in-medium [8] (upper solid line) or vacuum (dash-dotted line) vector-meson spectral functions, added to QGP radiation and the cocktail of hadronic decays after thermal freezeout (including correlated charm decays) [24], and compared to PHENIX data [23]. Right panel: studies of QGP emission [25] including an improved photon limit with EM spectral functions fitted to recent lattice-QCD computations [26] (middle solid lines) and variations in the equation of state (dashed line).

compared to SPS ($T_0 \simeq T_c$). However, in the low-mass region, the thermal dilepton yield is not very sensitive to the Boltzmann factor, but rather to the 4-volume of emission. The latter is much smaller in the QGP than in the hadronic phase, and this is the ultimate reason that QGP emission cannot compete with thermal hadronic emission at masses around 0.3 GeV. This is illustrated in the right panel of Fig. 5, where several attempts have been made to augment the QGP contribution. None of these reaches the size of the hadronic yield [25]. Thus, one is led to conclude that the origin of the PHENIX enhancement must be a “cool”, long-lived hadronic source with little flow (as dictated by the small slope of the corresponding q_t spectrum, $T_{\text{slope}} \simeq 100$ MeV). Together with further theoretical analysis, the upcoming PHENIX data for low-mass dileptons, which have been a priority of the recent RHIC run-10, will hopefully shed light on this “anomalous” excess.

Interesting results for dielectron spectra are also obtained at low energies, $E_{\text{lab}} = 1-2$ AGeV [27]. For light-ion projectiles (e.g., ^{12}C), the dominant role seems to be played by elementary processes, i.e., primordial N - N Bremsstrahlung and final-state Dalitz decays of η , $\Delta(1232)$, etc. Heavier projectile-target configurations are hoped to reveal the long-awaited results on vector-meson modifications in a low- T high- ρ_B medium.

THEORETICAL INTERPRETATION

Let us put the above findings into a broader perspective. Resonance melting in the medium is a general phenomenon. It is visible in cold nuclei, where photo-absorption spectra exhibit the disappearance of the second and third resonance region (recall left panel of Fig. 2; the $\Delta(1232)$ width is “protected” by Pauli blocking in the πN final state). Even the JLab data on the F_2^N structure function on the deuteron indicate a

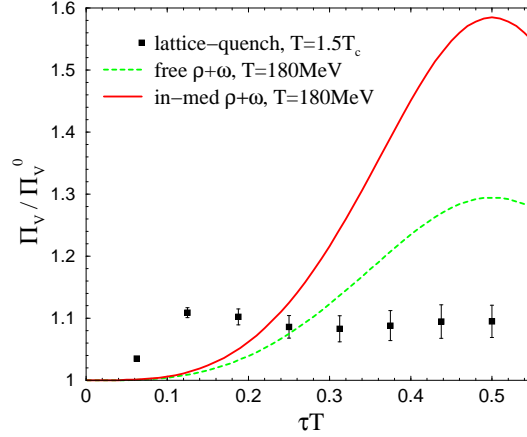


FIGURE 6. Euclidean correlator ratios in the vector channel for the hadronic many-body approach [8] as computed in Ref. [28], compared to lattice QCD data of Ref. [29].

“premature” approach to the general DIS scaling curve, i.e., at smaller Q^2 than on the proton [3]. The same mechanism may very well be at the origin of driving the timelike dilepton emission rate in hadronic matter toward the one from hard-thermal-loop (HTL) resummed perturbative QCD [22] (recall the right panel of Fig. 4). Note that the perturbative result is automatically chirally symmetric. Further constraints can be obtained from lattice QCD (IQCD) data for the euclidean correlator in the vector channel, which is related to the spectral function via

$$\Pi_V(\tau, q) = - \int_0^\infty \frac{dq_0}{\pi} g_{\mu\nu} \text{Im}\Pi_V^{\mu\nu}(q_0, q) \frac{\cosh[q_0(\tau - 1/2T)]}{\sinh[q_0/2T]}. \quad (2)$$

Recent IQCD results, after removal of a so-called zero-mode contribution, find good agreement with the HTL result (except at small q_0 where HTL does not apply) [26]. Figure 6 illustrates an early comparison [28] of the euclidean correlator ratio for in-medium ρ and ω spectral functions in the hadronic phase to quenched IQCD data [29] (the denominator, Π_V^0 , corresponds to the non-interacting $q\bar{q}$ continuum for u and d flavors). The agreement with the hadronic calculation improves for the recent, zero-mode subtracted, IQCD data (the zero-mode contribution is not present in the hadronic calculation). Progress is also being made in evaluating axialvector spectral functions in medium [30], as reported at this meeting [31]. A broadening found for the a_1 peak in nuclear matter supports a general tendency of “chiral restoration through broadening”.

CONCLUSIONS

Hadronic many-body calculations of vector-meson spectral functions are becoming a quantitative tool to perform spectral analysis of strongly interacting systems. Thus far, a strong broadening of the ρ -meson consistently describes available dilepton and photon emission data in elementary and heavy-ion reactions. The only exception at current are

the PHENIX low-mass dileptons, where a large QGP contribution is unlikely to resolve the discrepancy. In the absence of explicit measurements of the axialvector spectral function, conclusions on chiral restoration have to be inferred indirectly. Degeneracy of the in-medium hadronic vector correlator with chirally symmetric perturbative and lattice spectral functions can, in principle, close this gap. Intriguing connections to the spacelike regime, accessible at JLab, should be pursued further.

ACKNOWLEDGMENTS

I gratefully acknowledge my collaborators, specifically D. Cabrera, C. Gale, D. Jido, T.S.H. Lee, F. Riek, L. Roca, M. Urban, H. van Hees and J. Wambach. This work has been supported by the U.S. National Science Foundation under CAREER grant no. PHY-0449489 and under grant no. PHY-0969394, and by the A.-v.-Humboldt Foundation.

REFERENCES

1. C. Bonati *et al.*, *Phys. Rev. D* **81**, 085022 (2010).
2. K. Nakamura *et al.* [Particle Data Group], *J. Phys. G* **37**, 075021 (2010).
3. I. Niculescu *et al.*, *Phys. Rev. Lett.* **85**, 1182–1185 (2000).
4. R. Rapp, J. Wambach and H. van Hees, in *Relativistic Heavy-Ion Physics*, edited by R. Stock and Landolt Börnstein (Springer), New Series **I/23A**, 4-1 (2010); [arXiv:0901.3289[hep-ph]].
5. S. Leupold, V. Metag and U. Mosel, *Int. J. Mod. Phys. E* **19**, 147–224 (2010).
6. M. Urban *et al.*, *Nucl. Phys. A* **641**, 433–560 (1998); R. Rapp *et al.*, *Phys. Lett. B* **417**, 1–6 (1998).
7. M. Harada and K. Yamawaki, *Phys. Rept.* **381**, 1–233 (2003).
8. R. Rapp and J. Wambach, *Eur. Phys. J. A* **6**, 415–420 (1999).
9. M.H. Wood *et al.* [CLAS Collaboration], *Phys. Rev. C* **78**, 015201 (2008).
10. R. Arnaldi *et al.* [NA60 Collaboration], *Phys. Rev. Lett.* **96**, 162302 (2006).
11. D. Adamova *et al.* [CERES/NA45 Collaboration], *Phys. Lett. B* **666**, 425–429 (2008).
12. R. Arnaldi *et al.* [NA60 Collaboration], *Eur. Phys. J. C* **59**, 607–623 (2009); *ibid.* **61**, 711–720 (2009).
13. F. Riek *et al.*, *Phys. Lett. B* **677**, 116–120 (2009); *Phys. Rev. C* **82**, 015202 (2010).
14. Y. Oh and T.-S.H. Lee, *Phys. Rev. C* **69**, 025201 (2004).
15. T. Ishikawa *et al.*, *Phys. Lett. B* **608**, 215–222 (2005).
16. M. Kotulla *et al.* [CBELSA/TAPS Collaboration], *Phys. Rev. Lett.* **100**, 192302 (2008).
17. S. Damjanovic, R. Shahoyan and H.J. Specht [NA60 Collaboration], *CERN Cour.* **49N9**, 31 (2009).
18. H. van Hees and R. Rapp, *Nucl. Phys. A* **806**, 339–387 (2008).
19. K. Dusling and I. Zahed, *Phys. Rev. C* **80**, 014902 (2009).
20. J. Ruppert *et al.*, *Phys. Rev. Lett.* **100**, 162301 (2008).
21. E.L. Bratkovskaya, W. Cassing and O. Linnyk, *Phys. Lett. B* **670**, 428–433 (2009).
22. E. Braaten, R.D. Pisarski and T.C. Yuan, *Phys. Rev. Lett.* **64**, 2242 (1990).
23. A. Adare *et al.* [PHENIX Collaboration], *Phys. Rev. C* **81**, 034911 (2010).
24. A. Toia, private communication.
25. R. Rapp, work in progress (2010).
26. F. Karsch *et al.*, Proceedings of Lattice 2010, to be published.
27. G. Agakishiev *et al.* [HADES Collaboration], *Phys. Lett. B* **690**, 118–122 (2010).
28. R. Rapp, *Eur. Phys. J. A* **18**, 453–462 (2003).
29. F. Karsch *et al.*, *Phys. Lett. B* **530**, 147–152 (2002).
30. D. Cabrera *et al.*, *Prog. Theor. Phys.* **123**, 719–742 (2010).
31. L. Roca, these proceedings.